ACS APPLIED MATERIALS & INTERFACES

Research Article

www.acsami.org

Field Effect Transistors Based on Polycyclic Aromatic Hydrocarbons for the Detection and Classification of Volatile Organic Compounds

Alona Bayn,[†] Xinliang Feng,[‡] Klaus Müllen,[‡] and Hossam Haick*,[†]

[†]The Department of Chemical Engineering and the Russell Berrie Nanotechnology Institute, Technion − Israel Institute of Technology, Haifa 3200003, Israel

[‡]Max-Planck-Institute for Polymer Research, Postfach 3148, D-55021 Mainz, Germany

Supporting Information

ABSTRACT: We show that polycyclic aromatic hydrocarbon (PAH) based field effect transistor (FET) arrays can serve as excellent chemical sensors for the detection of volatile organic compounds (VOCs) under confounding humidity conditions. Using these sensors, w/o complementary pattern recognition methods, we study the ability of PAH-FET(s) to: (i) discriminate between aromatic and non-aromatic VOCs; (ii) distinguish polar and non-polar non-aromatic compounds; and to (iii) identify specific VOCs within the subgroups (i.e., aromatic compounds, polar non-aromatic compounds, non-polar non-aromatic compounds). We further study the effect of water vapor on the sensor array's discriminative ability and derive patterns that are stable when exposed to different constant values of background humidity. Patterns based on different independent electronic features from an array of PAH-FETs may bring us one step closer to creating a unique fingerprint for individual VOCs in real-world applications in atmospheres with varying levels of humidity.

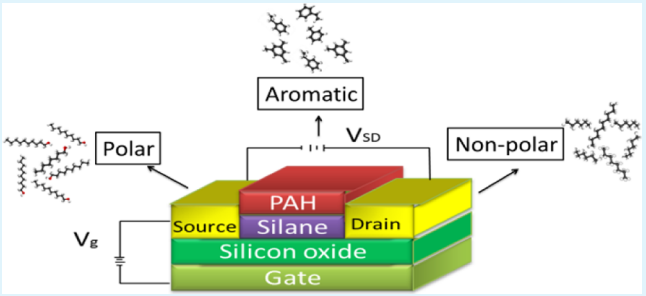

KEYWORDS: *polycyclic aromatic hydrocarbon, sensor, volatile organic compound, humidity, field effect transistor, detection*

INTRODUCTION

Volatile organic compounds (VOCs) tend to evaporate easily at room temperature. Many VOCs are associated with emissions from industrial processes (e.g., heating oil, aldehydes, alcohols), transportation (e.g., gasoline, diesel, kerosene), and use of organic solvents (e.g., benzene, butadiene, hexane, toluene, xylene, acetone) that are in part toxic or carcinogenic.[1,2] Furthermore, several VOCs associated with metabolic and/or pathophysiologic processes have been used for diagnosing a wide variety of diseases, including, but not confined to, lung cancer,[3−11] head and neck cancer,[9] liver metastasis,[12] kidney disease,[13,14] Parkinson's disease and Alzheimer's disease,[15,16] and multiple sclerosis.[17]

Detection of VOCs is generally achieved by means of gas sensors.[18] Although highly selective sensors do exist for a limited number of substances (e.g., hydrogen sulfide, phosphine), such gas sensors are very sensitive to cross-interfering substances and provide an overall result in response to a general class or group of chemically related contaminants. These gas sensors provide a single collective reading for all of the detectable substances present in the surrounding environment at any moment, but they cannot distinguish different contaminants they are able to detect. Additionally, such gas sensors are highly affected by the humidity in the environment examined.[19−21] Varying levels of humidity are a serious obstacle in the application of such gas sensors, causing different responses and leading to a decrease in the selectivity toward the targeted analytes. Interaction water molecules and the charge carriers in the semiconductor as well as their diffusion in grain boundaries[22] causes a change in the intermolecular interactions. In some cases, the influence of water associated ions and molecules changes the work function and morphology of the semiconductor.[23] All the mechanisms noted affect the electrical behavior of the sensor. The higher the humidity levels, the higher the deterioration effect of the sensors. There have been many attempts to overcome this complication. Representative examples include the use of sensing materials that are not affected by changes in humidity, or the use of several sensors reacting differently to water vapor in order to calibrate the response to the analyte alone.[19] Unfortunately, the proposed approaches are applied on a sensor created to identify one specific analyte. When dealing with an array of different sensors meant to recognize a number of complex compounds, these approaches are harder to implement.[24] A novel solution to the humidity problem suggested using FRID wireless sensors that provide a reliable response in the presence of various humidity levels by a multivariate analysis from a single sensor correcting the humidity effect. Nevertheless, wireless sensor networks are relatively new technology; thus, problems in maintenance, routing, and coverage may present a challenge.[25]

Received: February 6, 2013
Accepted: March 19, 2013
Published: March 19, 2013

   dx.doi.org/10.1021/am4005144 | ACS Appl. Mater. Interfaces 2013, 5, 3431−3440

With this in mind, a simple and easy-to-use array of sensors that is minimally affected by counteracting humidity background is definitely needed.

To achieve chemical sensors with low sensitivity to humidity, we have recently exploited polycyclic aromatic hydrocarbon (PAH) derivatives.[26−29] PAH derivatives with hydrophobic terminations produced a hydrophobic surface that effectively counteracted the sensitivity to humidity, enabling detection of traces of VOCs even in high humidity environments (~80% relative humidity).[26−29] In a series of preliminary studies, hybrid structures containing PAH layers on top of a quasi 2D network of single wall carbon nanotubes (SWCNTs) have shown excellent detection and classification of VOCs under both low and high humidity backgrounds. In these devices, the PAH derivatives served as an electrically insulating adsorption phase for VOCs, while the SWCNTs served as the sole pathway for translating and transferring the PAH−VOC interactions to electrical signals. Using this architecture, Zilberman et al. found that both the PAH corona and the organic functionalities of these molecules contribute to the chemical sensing of the VOCs.[27] For instance, the PAH corona, made of condensed aromatic rings, interacts strongly with the phenyl rings of aromatic hydrocarbons (e.g., ethyl benzene), while the detection of OH-terminated (polar) VOCs is promoted by the presence of oxygen in the substituent functionality.[27] Nevertheless, in this architecture, the affinity of the PAH derivatives toward the VOCs of interest can be finely tuned by proper selection of the (synthetically designed) PAH derivative structures—a process that requires continuous synthetic skills and efforts. Additionally, the involvement of a random network of SWCNTs might lead to relatively high production costs and might delay the implementation of the PAH-based sensors in the well-established VLSI industry and/or production lines.

In this paper, we present a technology based on an array of field effect transistors (FETs) coated with a layer of different (semi)conducting PAHs, without the involvement of any other (e.g., SWCNT) conductive layer. PAH molecules are able to self-assemble into long molecular stacks with a large, electron-rich, semiconducting core, guaranteeing good charge carrier transport along the molecular stacking direction and a relatively insulating periphery.

We investigate the possibility of using PAH-FETs as a fast, noninvasive portable technology that can be used for the widespread detection of various VOCs. In this endeavor, we examine the use of different electrical features extracted from a single sensor to increase the chances of correct identification (cf. refs 30 and 31). On the basis of these results, we explore the optimal ways to utilize independent electrical parameters (e.g., threshold voltage, mobility, current-on/current-off ratio) of PAH-FETs for the classification of various VOCs in a humid atmosphere while employing the analysis on an array of different sensors with improved sensitivity and selectivity towards important VOCs. We show that a combination of different electrical parameters, extracted from a single PAH-FET or from several devices, can be used as an array of virtual sensors.

EXPERIMENTAL SECTION

Device Preparation. Back-gated PAH-FETs were deposited on a p-type Si(100) wafer covered with a 300 nm thick thermally grown SiO_2 field oxide layer (Figure 1a). Ten pairs of interdigitated Au/Ti electrodes with a circular geometry (overall radius of 1500 μm) were deposited on top of the SiO_2 layer, and an aluminum back gate was

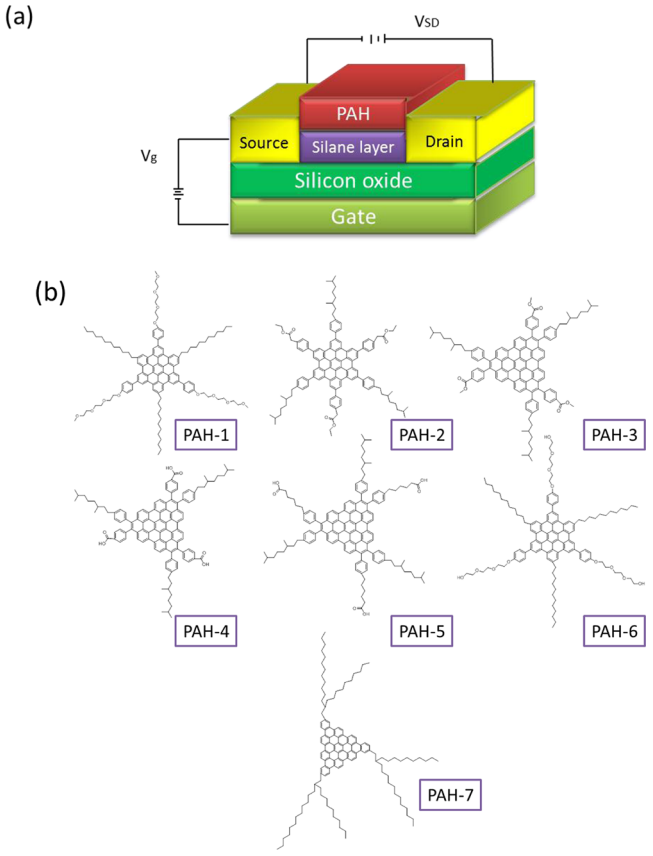

Figure 1. (a) Schematic representation of the sensor structure. (b) Schematic drawing of the chemical structures of all PAHs tested in this study.

deposited on the backside of the Si substrate after removal of the oxide from the back of the wafer. The width of each electrode was 5 μm, the thickness of each electrode was 250 nm, and the distance adjacent electrodes was 25 μm. The SiO_2 surface electrodes was functionalized with a hexyltrichlorosilane (HTS) monolayer using the two-step amine-promoted procedure described elsewhere.[32−37] Similar devices without the HTS layer were fabricated as controls. The HTS-terminated and pristine SiO_2 surfaces were spray-coated with different PAH films that were chosen from a reservoir of seven PAH derivatives (see Figure 1b and Table 1). The synthesis of PAH-1,[38] PAH-2,[39] and PAH-7[40] has been described in previous works. The synthesis of PAH-3 to PAH-6 will be described elsewhere. The PAH layer was spray-coated from a 50 μL 10^{-3} M solution (PAH-2, PAH-3, and PAH-7 in toluene; PAH-4 in tetrahydrofurane), after which the devices were dried overnight in a 100 °C oven, to evaporate possible residual

Table 1. Structural Properties of All the PAH Derivatives Studied in the Experiments

PAH derivative	aromatic-core shape	no. of carbon atoms in the core	side group	side group polarity
PAH-1	hexagonal	42	ether	weak polar
PAH-2	hexagonal	42	ester (ethyl)	strong polar
PAH-3	semi-triangular	48	ester (methyl)	strong polar
PAH-4	semi-triangular	48	carboxyl	strong polar
PAH-5	semi-triangular	48	carboxyl	strong polar
PAH-6	hexagonal	42	alcohol (hydroxyl)	strong polar
PAH-7	triangular	60	alkyl chain	non-polar

dx.doi.org/10.1021/am4005144 | ACS Appl. Mater. Interfaces 2013, 5, 3431−3440

solvents in the PAH layer. Layer morphology and surface coverage were studied by scanning electron microscopy (SEM).

Electrical FET Characterization in Air. A probe station that is connected to a device analyzer (Agilent B1500A) was used to collect the electrical signals of the sensors in ambient air. Voltage-dependent back-gate measurements (I_{ds} vs V_g), swept backward and forward between −40 and 40 V with 500 mV steps and at 30 V source-drain voltage (V_{ds}), were used to determine the performance of the PAH-FET devices.

Sensing Volatile Organic Compounds. The PAH-FETs were exposed to three groups of VOCs: alcohols (decanol and octanol), alkanes (hexane, decane, and octane), and aromatic compounds (mesitylene, styrene, ethyl benzene, and toluene). All compounds were purchased from Sigma-Aldrich Ltd. (Israel) and Fluka Ltd. (Israel), having >99% purity and <0.001% water. Oil-free purified air, obtained from a compressed air source, that had a baseline RH (relative humidity) of 5.0 ± 0.2% and an organic contamination of <0.3 ppm (measured by a commercial PID detector - ppbRAE 3000), was used as a carrier gas for the analytes and as a reference gas. The vapor of the analytes was created by a bubbler system that uses glass bubblers, holding the analytes in liquid states. The saturated analyte vapor from the bubblers was diluted with different flow rates of air to create different concentrations. The relative humidity (RH) was regulated by a combination of dry air (5% RH) and water saturated vapor (100% RH). The partial pressure of analyte vapors was changed between p_a/p_0 = 0.05, 0.1, and 0.2 (p_a stands for the partial pressure of the analyte, and p_0 stands for the saturated vapor pressure at 20 °C) in an environment of 5−40% RH. Unless otherwise stated, we focus our presentation on analytes at p_a/p_0 = 0.1 in an environment of either 5 or 40% RH. The exposures were performed as follows: (i) exposure to dry air (5% RH) for 30 min; (ii) exposure to VOC(s) for 20 min; and (iii) cleaning the sensor surrounding with dry air for another 30 min. Two repetitions per exposure were performed to ensure the reproducibility of the responses. The electrical measurements of the PAH-FETs were conducted using a homemade exposure system. The sensors developed were placed on a circuit board inside a stainless steel exposure chamber. The electrical response of the sensors was measured by a Keithley 2636A system SourceMeter and Keithley 3706 system Switch/Multimeter. S/D (S-source, D-drain) current (I_{ds}) versus voltage dependent back-gate (V_g) measurements, swept backward between +40 and −40 V with 200 mV steps and at V_{ds} = 30 V, were performed.

Data Analysis. Four device features were extracted from each sensor: (i) I at V_g = −20 V, the current value at gate voltage of −20 V; (ii) μ_h, hole mobility values extracted from the I_{ds} vs V_g curve; (iii) V_{th}, voltage threshold; (iv) $I_{on/off}$, the ratio current-on (I_{on}), and current-off (I_{off}). Each device feature was plotted as a function of exposure time to a specific analyte and normalized response was then extracted (see "Sensing of VOCs with PAH-FETs" below section for more details). The four normalized sensing features examined in the present work were (i) $\Delta I/I_0$, normalized current (at V_g = −20 V); (ii) $\Delta\mu_h/\mu_{h0}$, normalized mobility; (iii) $\Delta V_{th}/V_{th0}$, normalized voltage threshold; and (iv) $\Delta I_{on/off}/I_{on/off0}$, normalized on−off ratio of the current. Discrimination various VOCs was achieved with the help of discriminant factor analysis (DFA).[15−17] Statistical tests were performed by SAS JMP, version 8.0. The program input consisted of various electronic features from each sensor deduced from the exposure experiments.

RESULTS AND DISCUSSION

Preliminary FET Device Characterization in Ambient Air. Figure 1a shows a schematic illustration of the PAH-FETs tested. Two sets of FETs were prepared as described in the Experimental Section. The first set incorporated HTS-passivated field oxide layers; the second set was fabricated using pristine oxide layers. Each of the two sets included devices based on the seven PAH molecules shown in Figure 1b. The properties of the molecules are listed in Table 1. Each device was fabricated in duplicate.

The outline of the work is represented by the flowchart in Figure 2. The first step was the choice of the most suitable PAH molecules for optimal FET performance. Measurements of I_{ds} vs V_g in ambient air (RH ∼ 40%), swept backward and forward between −40 and 40 V at V_{ds} = 30 V, showed that layers based on PAH-2, -3, -4, and -7 molecules yielded clearly superior devices than layers based on PAH-1, -5, and -6. The signal-to-noise ratios for the former four molecules exceeded 13, whereas the latter three molecules yielded signal-to-noise ratios below 10. Furthermore, the average hysteresis between backward and forward back-voltage sweep (another important quality measure for FET sensors, which should be as small as possible, see below) was sufficiently small (<4 V) for sensing applications in ambient atmosphere in devices based on PAH-1, -5, and -6 but excessively large (>15 V) for the devices based on PAH-1, -5, and -6. In some of the measurements, the electrical features of PAH-1, -5, and -6 could not even be extracted from the current vs voltage curve, due to the lack of a clear field effect behavior. Consequently, we have performed the subsequent device characterization and the sensing experiments only on the devices based on PAH-2, -3, -4, and -7.

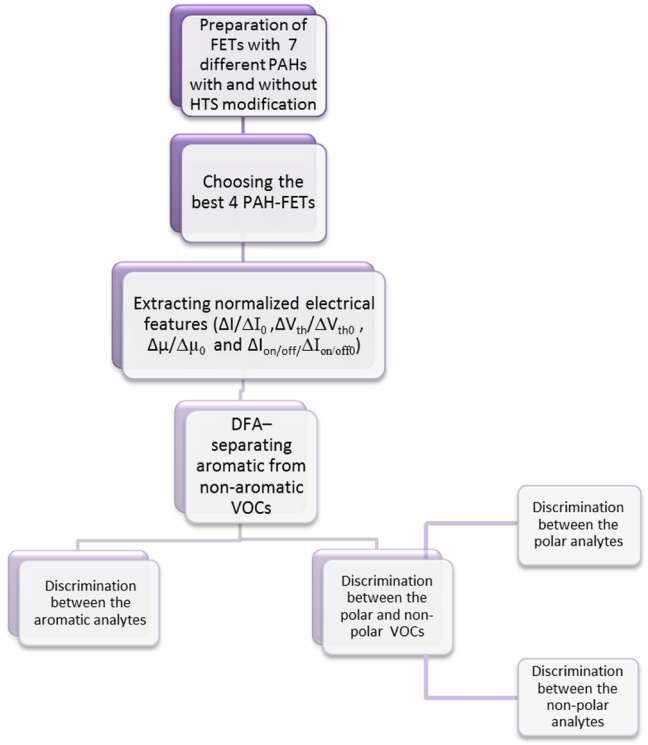

Figure 2. Flowchart representing the steps in analysis of the discriminative ability of the PAH FET array.

Surface Morphology and Surface Coverage of the PAH-FETs. Figure 3 presents scanning electron microscopy (SEM) images of the PAH-2, -3, -4, and -7 layers covering the HTS-passivized FET devices. As seen in the figure, films made of different PAH molecules exhibited substantial differences in surface coverage and morphology. Substantial differences in surface coverage and morphology were observed different molecules. PAH-2 has a surface coverage of 57.4 ± 15% (see Figure 2a); PAH-3 has a surface coverage of 66.9 ± 11% (see Figure 2b); PAH-4 has a full surface coverage and a smooth

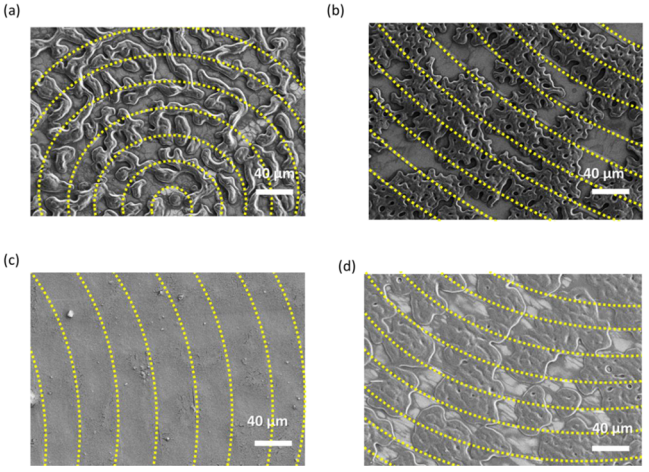

Figure 3. Scanning electron microscopy images of the FET surface that is covered with (a) a PAH-2 layer, (b) a PAH-3 layer, (c) a PAH-4 layer, and (d) a PAH-7 layer, as prepared from 10^{-3} M PAH solutions, before exposure to analytes. The positions of the 5 μm wide interdigitated electrodes are highlighted by dashed yellow lines. The images were obtained with a secondary electron detector.

layer (see Figure 2c); and PAH-7 has a surface coverage of 71.2 ± 5% (see Figure 2d). The incomplete coverage of the PAH-2, PAH-3, and PAH-7 films did not prevent efficient electrical transport source and the drain, due to the formation of multiple continuous PAH pathways adjacent islands as well as source and drain electrodes. The morphology of the various PAH films remained constant throughout the entire study. Neither exposure to analytes nor humidity conditions changed the morphology of the PAH films (cf. Figure 3 and Figure S1, Supporting Information).

The Effect of the Silane Layer on the Electronic FET Properties. The hysteresis that is typically observed between backward and forward back-voltage sweep forms one of the major obstacles to using FETs as gas sensors. The hysteresis is defined as the gap forward and backward electrical response in source-drain current while changing the back gate voltage.[35] The following explanation has been proposed: the silicon oxide (SiO_2) surface allows the formation of surface trap states (Si–OH, Si–O^-, Si–OH^{2+} species)[41] that can function as sorption sites and, therefore, capture water molecules. When the relative humidity of the environment is high enough, water drops condensate on the SiO_2 surface and are ionized. The resulting considerable changes in the FET characteristics are prone to masking the mild changes in the current induced by the targeted analyte(s). Note that the SiO_2 surface was extremely relevant to our case, since PAH-2, PAH-3, and PAH-7 layers did not cover the entire oxide layer.

Here we have investigated the feasibility of HTS surface modification as a way to remove the trap states from the SiO_2 surface, reducing the hysteresis effect. This approach has been proven as an efficient way to reduce the tap states (mainly Si–OH groups) on the SiO_2 surface, thus enhancing their related electrical and sensing features.[33,35]

It should be noted that only the SiO_2 was covered with the HTS molecules but not the electrodes. Hence, the semiconducting PAH layers were in direct contact with the source and drain metal electrodes. Figure 4 and Table 2 show that the HTS surface modification improved almost all electrical features of the PAH-FETs studied. All examined devices exhibited higher on-current/off-current ($I_{on/off}$) ratio, indicating

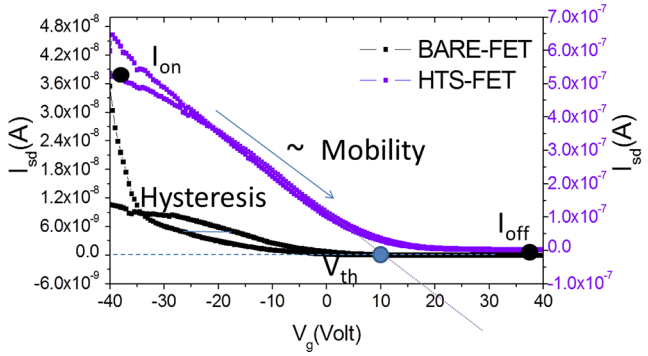

Figure 4. Linear characteristics of the source-drain current (I_{ds}) vs gate voltage (V_g) of the FET covered in a PAH-2 layer with (purple curve) and without (black curve) a HTS layer at the interface. The measurements were carried out by a forward and backward scan of V_g steps of 500 mV, at V_{sd} = 30 V.

an improvement in the electrical efficiency of the FET device. Note, however, that higher values of $I_{on/off}$ do not necessarily imply enhancement in the sensitivity and selectivity for sensing applications. All examined PAH-FET devices exhibited elevated values of carrier mobility, indicating an improvement in the conductivity of the charge carrier tunnel. FETs that were covered with discontinuous layers of PAH-2, PAH-3, or PAH-7 exhibited negative V_{th} without the HTS modification and positive V_{th} with the HTS modification, meaning that the p-type device (that usually conducts current in the negative values of gate voltage) is open over a wider range of voltages. On the other hand, the FETs that were covered with continuous layers of PAH-4 exhibited positive V_{th} without the HTS modification and negative V_{th} with the HTS modification. In this device, the HTS seems to increase the resistance gate and the semiconducting PAH-4 layer. Of great importance, the addition of the HTS modification has shown a clear effect on the hysteresis of the examined devices, in the following order: PAH-2 < PAH-4 < PAH-3 < PAH-7. PAH-2 with HTS modification has shown the smallest hysteresis and, hence, is the least sensitive to water.

Sensing of VOCs with PAH-FETs. FETs covered with PAH-2, PAH-3, PAH-4, and PAH-7 layers were exposed to several representative analytes from three chemical groups (alcohols, alkanes, and aromatic compounds). The analytes and their physical and chemical properties are listed in Table 3. The gate voltage (V_g) was swept from −40 to 40 V at V_{ds} = 30 V. The following electrical features were extracted: (i) I at V_g = −20 V, the current value at a gate voltage of −20 V; (ii) μ_h, hole mobility values extracted from the I_{ds} vs V_g curve, using the following equation:

$$\mu_h = \frac{L}{ZC_i}\frac{1}{V_{ds}}\frac{\partial I}{\partial V_g} \quad (1)$$

where L is the length of conductive channel, Z is the width of the conductive channel, V_{ds} is the voltage applied source and drain electrodes, C_i is the capacitance per unit area of the silicon oxide layer, I is the current, and V_g is the voltage applied on the gate electrode; (iii) V_{th}, voltage threshold calculated by extrapolating the linear part of the I_{ds} vs V_g curve and extracting the interception value with the voltage axis (see Figure 4); (iv) $I_{on/off}$, the ratio on-current (I_{on}) and off-current (I_{off}), calculated by dividing the current value when the device is "open" (i.e., I_{on})—an average of five measurements of current ending with V_g = −40 V—by the value when the device is

dx.doi.org/10.1021/am4005144 | ACS Appl. Mater. Interfaces 2013, 5, 3431−3440

Table 2. Electrical Features of the Different PAH-FET Devices, with and without the Silane (HTS) Surface Modification

	I_{on}/I_{off}		V_{th} (V)		hysteresis[a] (V)		mobility ($cm^2 V^{-1} s^{-1}$)	
	bare FET	HTS-FET	bare FET	HTS-FET	bare FET	HTS-FET	bare FET	HTS-FET
PAH-2	223 ± 20.5%	381 ± 23.3%	−4.00 ± 44.2%	10.0 ± 53.8%	10.0 ± 25.7%	1.50 ± 55.6%	$(0.10 \times 10^{-6}) \pm 24.2\%$	$(0.36 \times 10^{-5}) \pm 33.7\%$
PAH-3	1430 ± 22.8%	27300 ± 27.8%	−13.0 ± 5.4%	8.00 ± 3.2%	5.50 ± 35.6%	2.00 ± 33.3%	$(0.24 \times 10^{-6}) \pm 54.6\%$	$(0.14 \times 10^{-4}) \pm 64.5\%$
PAH-4	134 ± 33.5%	281 ± 26.6%	7.00 ± 17.1%	8.00 ± 14.3%	12.0 ± 22.4%	3.00 ± 16.7%	$(0.13 \times 10^{-6}) \pm 10.7\%$	$(0.69 \times 10^{-6}) \pm 5.7\%$
PAH-7	451 ± 24.9%	1930 ± 17.8%	−3.00 ± 6.1%	16.0 ± 7.9%	10.0 ± 11.9%	7.00 ± 15.9%	$(0.09 \times 10^{-6}) \pm 60.5\%$	$(0.50 \times 10^{-6}) \pm 63.2\%$

[a]Hysteresis is represented by the largest distance (in the same current value) curves of the forward and backward current on the gate voltage axes.

"closed" (i.e., I_{off})—an average of five measurements of current starting with V_g = +40 V. For the final analysis, normalized values of each extracted electrical feature were obtained by dividing the sensor's steady state value under analyte exposure by the baseline value. According to the following equation:

$$\text{normalized feature} = \frac{\Delta r}{r_0} = \frac{r_1 - r_0}{r_0} \quad (2)$$

where r_0 is an average of five measurements at the end of the air exposure step and r_1 is an average of five measurements at the end of an analyte exposure step. A representative example of the normalized sensing feature ($\Delta r/r_0$) as a function of time is presented and discussed in Figure S2 of the Supporting Information.

Figure 5a and b shows the normalized current, $\Delta I/I_0$, under exposure to different analytes in 5% RH environment. Most responses are negative. Certain trends were identified, for example, the responses of PAH-2 and -3 (5% RH) to the aromatic analytes scaled with the analytes' polarity: the higher the polarity of the analyte, the greater the decrease in normalized current. In general, we can see that the absolute responses of all four sensors to the exposure with aromatic VOCs were higher than those to the exposure with non-aromatic VOCs. By comparing the normalized current responses obtained under 5 and 40% RH (see Figure 5a and c), we found that the effect of the humidity background was considerable on the FETs based on PAH-3 and PAH-4: neither the values, the direction of the change, nor the trend of the response were similar changing environments. For FETs based on PAH-2 and PAH-7 films, the changes were less drastic: the responses on exposure to VOCs fewer than 5% RH were slightly diminished when the humidity of the background increased to 40% RH, but the general trends were not changed.

Figure 6 presents the normalized mobility, $\Delta\mu_h/\mu_{h0}$, of the sensors under VOC exposure. Most of the exposures resulted in a decrease in $\Delta\mu_h/\mu_{h0}$. PAH-2 and PAH-3 exhibited only a decrease in $\Delta\mu_h/\mu_{h0}$ in both low (5%) and high (40%) relative humidity (RH) environments. On the other hand, PAH-4 and PAH-7 showed both an increase and decrease, depending on the types of the exposed VOC and RH level. Another noticeable fact is that PAH-2 and PAH-3 displayed lower standard deviations, compared with PAH-4 and PAH-7. PAH-2 and PAH-3 discriminated well various VOCs based on the $\Delta\mu_h/\mu_{h0}$ alone. PAH-2 is of special interest, since the discrimination ability of this device was not (or minimally) affected by the RH level of the exposure environment. Indeed, neither the response magnitude nor the ratio responses obtained on exposure to various VOCs was affected. In the category of aromatic VOCs exposed to PAH-2 and -3, a disproportional relationship was found $\Delta\mu_h/\mu_{h0}$ (mesitylene < toluene < styrene < ethyl benzene) and the VOC polarity, both at low and high RH levels (see Figure 6): the higher the polarity, the lower the $\Delta\mu_h/\mu_{h0}$. An exception was the response of PAH-2 to toluene. It is likely that the toluene adsorbed quite strongly to the PAH-2 surface, leaving significant residues within the sensing film during the cleaning process with dry air. The substantial decrease in $\Delta\mu_h/\mu_{h0}$ on exposure to aromatic VOCs could be related to one or both of the following reasons: (i) the aromatic VOCs have a higher bonding strength to the surface, having a greater effect on the charge carrier's mobility, perhaps due to swelling of the PAH layers; (ii) the higher absorption ability of aromatic VOCs causes a greater dipole-

Table 3. Physical and Chemical Properties of the VOCs Used as Analytes for the Exposure Experiments

VOC	formula	p_0 (kPa @ 20 °C)[a]	dipole moment (D)	density (g·cm^{-3})	molecular weight (g·mol^{-1})
hexane	$CH_3(CH_2)_4CH_3$	17.6	0	0.655	86.2
octane	$CH_3(CH_2)_6CH_3$	1.47	0	0.703	114
decane	$CH_3(CH_2)_8CH_3$	1.58	0	0.730	142.2
octanol	$CH_3(CH_2)_7OH$	0.114	2.00	0.824	130
decanol	$CH_3(CH_2)_9OH$	0.0148	1.68	0.830	158.3
mesitylene	$C_6H_3(CH_3)_3$	0.230	0	0.864	120
styrene	$C_6H_5CH{=}CH_2$	0.670	0.130	0.909	104
ethyl benzene	$C_6H_5{-}C_2H_5$	0.900	0.240	0.867	106
toluene	$C_6H_5{-}CH_3$	3.80	0.360	0.866	92.1

[a] p_0 stands for the VOC's vapor pressure at 20 °C.[42]

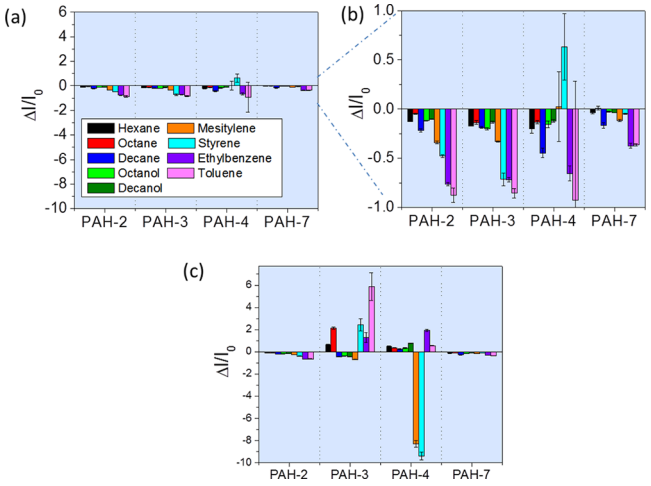

Figure 5. Normalized current (at $V_g = -20$ V) ($\Delta I/I_0$) while exposing the devices to different analytes at a concentration of $p_a/p_0 = 0.1$ in an environment of (a) 5% RH, (b) 5% RH (magnification), and (c) 40% RH. Each value is the average of two repeated exposures under the same conditions.

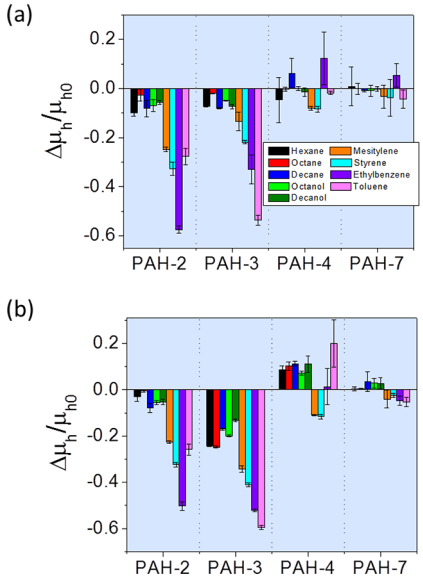

Figure 6. Normalized mobility ($\Delta\mu_h/\mu_{h0}$) values while exposing the devices studied to different analytes in an environment of (a) 5% RH and (b) 40% RH. The concentration in both figures is $p_a/p_0 = 0.1$. Each value is the average of two repeated exposures under the same conditions.

induced field than the other groups of VOCs (alcohols and alkanes), interfering with the field caused by the gate electrode. No relationship was found $\Delta\mu_h/\mu_{h0}$ and the polarity of non-aromatic VOCs.

PAH-3 and PAH-4 have the same aromatic core (semi-triangle) and organic side chains but slightly differ in the termination groups of the organic side chains (ester group in PAH-3 and carboxylic group in PAH-4). Integrating PAH-3 and PAH-4 in FET platforms exhibited substantially different $\Delta\mu_h/\mu_{h0}$ on exposure to the same conditions. This observation stresses the importance of the PAH's side chain for sensing applications. Side chains mediate the interaction VOC and the charge carrier channel of the organic semiconductor. They also play an important role in the self-assembly and morphology of the PAH on the surface—another reason for the discrepancies in the sensing characteristics of the sensors. The PAH-7 sensor exhibited responses at the order of, or lower than, the experimental variance(s) of the sensing measurements. Therefore, no clear relationship between the $\Delta\mu_h/\mu_{h0}$ and VOC characteristics could be established. Looking at Figures 5 and 6, we see that $\Delta I/I_0$ and $\Delta\mu_h/\mu_{h0}$ of each sensor has distinctive individual behavior as a result of the exposure, varying from analyte to analyte and also changing with the humidity levels. These variations give us the variability we need in the array of sensors as a whole, to discriminate between different analytes.

Figure 7 shows the effect of analyte exposure in different background humidity on the $\Delta V_{th}/V_{th0}$. PAH-2 exhibited the highest variability of response, in both high and low humidity: the responses to toluene and ethyl benzene (two of the most polar analytes) were 1 order of magnitude higher than those to the remaining analytes. The values of normalized V_{th} were positive under dry conditions. However, under 40% RH, PAH-4 showed negative responses to some analytes. No substantial other trends were noticed, but we can conclude that the $\Delta V_{th}/V_{th0}$ is very sensitive to humidity changes in the environment.

Figure 8 presents the normalized ratio averaged current when the channel is open (I_{on}) and closed (I_{off}). As seen in the figure, the experimental error is usually higher than the response value per se. These results imply that $\Delta I_{on/off}/I_{on/off0}$ cannot serve as a sensing feature, at either low or high RH levels. Therefore, the $\Delta I_{on/off}/I_{on/off0}$ feature was not included in the subsequent DFA analysis. As previously seen in Figure S2d of the Supporting Information, the response of the $I_{on/off}$ (even before normalization) does not give any reliable information. These high variances are caused by the inconsistent and noisy values for the off-current ranging from 1×10^{-13} to 8×10^{-11} A. The low values of the I_{off} are difficult to measure in the system used. In future exposure experiments, we can try to measure with a

dx.doi.org/10.1021/am4005144 | ACS Appl. Mater. Interfaces 2013, 5, 3431−3440

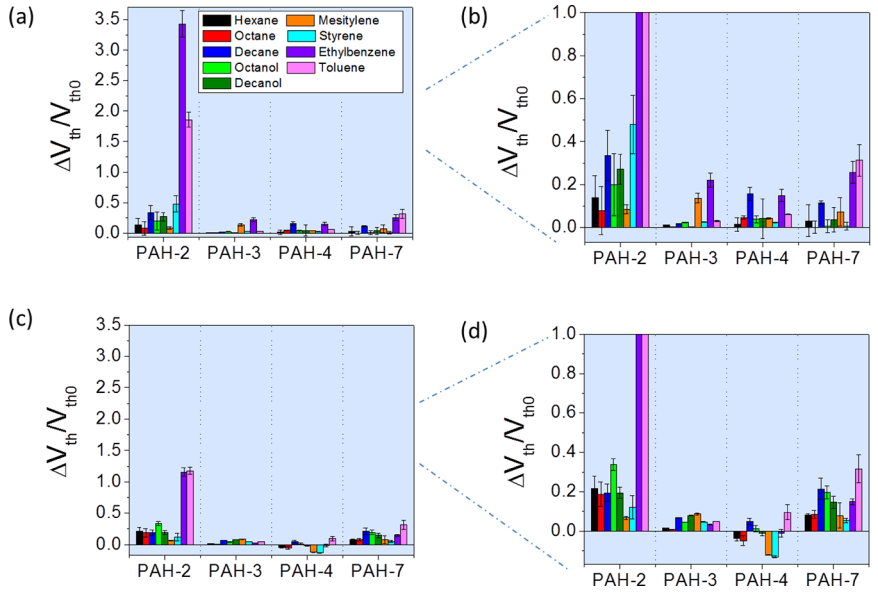

Figure 7. Normalized threshold voltage ($\Delta V_{th}/V_{th0}$) during exposure to different analytes in an environment of (a) 5% RH and (c) 40% RH. Parts b and d are the magnifications of parts a and b. The concentration in both figures is $p_a/p_0 = 0.1$. Each value is the average of two repeated exposures under the same conditions.

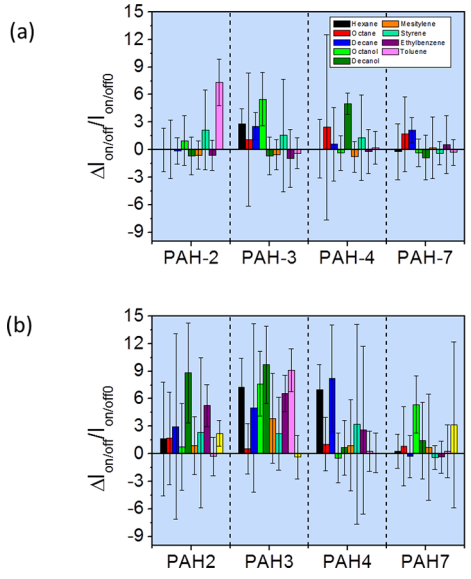

Figure 8. Normalized ratio averaged current when the device is open (I_{on}) and the value when the device is closed (I_{off}). The values calculated from the different sensors while exposing the device to different analytes in an environment of (a) 5% RH and (b) 40% RH. Each value is the average of two repeated exposures under the same conditions.

more sensitive system, or this noisy I_{off} can be replaced by the I_{on} value.

VOC Sensing Using Patterns from Combinations of Sensing Features. Discriminant factor analysis (DFA) was employed for effectively discriminating between (i) aromatic and non-aromatic VOCs; (ii) polar and non-polar analytes; and (iii) the studied VOCs in each subgroup, as shown in Figure 2. To evaluate the accuracy of differentiation, we also investigated other combinations of normalized features (of equal number) and estimated their accuracies according to the leave-one-out method.

Figure 9 presents a DFA map separating between aromatic and non-aromatic VOC groups. A high separation accuracy

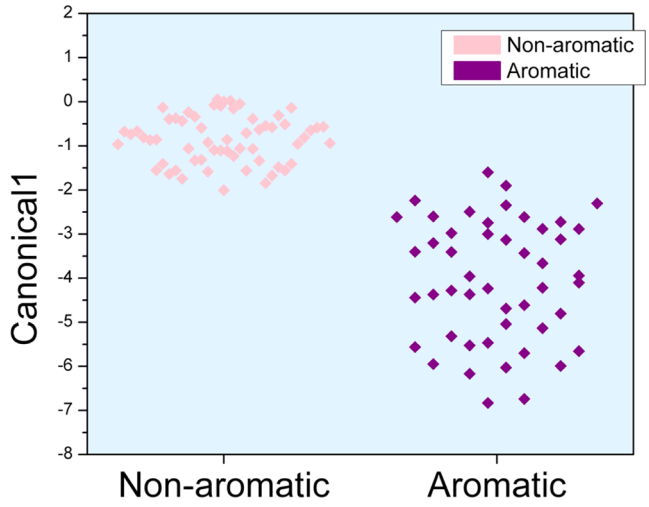

Figure 9. DFA results separating the non-aromatic (octanol, decanol, hexane, octane, decane) and aromatic VOCs (mesitylene, styrene, ethyl benzene, toluene) at different concentrations (p_a/p_0 = 0.05, 0.1, 0.2), both in 5% and in 40% RH. Each value is the average of two repeated exposures under the same conditions.

(using the leave-one-out method) of 95.37% was achieved, using only one variable, namely, $\Delta\mu_h/\mu_{h0}$, of the PAH-2 sensor. A single sensor provided us with a highly accurate separation, despite the fact that the VOCs were tested under different humidity conditions and at different concentrations. The fact that the separation is based on PAH-2 matches the conclusions that PAH-2 is least sensitive to water/humidity. Hence, PAH-2 made it possible to separate between VOCs according to their chemical or physical properties, irrespective of the confounding humidity. Table S1 of the Supporting Information illustrates the advantage of PAH-2 over the other sensors: PAH-2 gives the highest accuracy of separation compared to other sensors.

dx.doi.org/10.1021/am4005144 | ACS Appl. Mater. Interfaces 2013, 5, 3431−3440

The choice of the $\Delta\mu_h/\mu_{h0}$ is also not coincidental, because the $\Delta\mu_h/\mu_{h0}$ of PAH-2 gives significantly different values when exposed to aromatic analytes compared to non-aromatic ones and is less affected by changes in the humidity (see Figure 6). Additionally, the aromatic cluster is less well-defined than the cluster of the non-aromatic analytes (see Figure 9). Using only one sensor is of great significance for future applications, ensuring easy device fabrication and use as well as simple analysis.

Next, we distinguished the polar and non-polar non-aromatic compounds. The results are represented in Figure 10. We used different combinations of three sensing features from four PAH-FETs: $\Delta I/I_0$ of PAH-2, -3, -4, and -7; $\Delta\mu_h/\mu_{h0}$ of PAH-4 and -7; and $\Delta V_{th}/V_{th0}$ of PAH-3 and -7. The accuracy of separation received by the leave-one-out method is 80%.

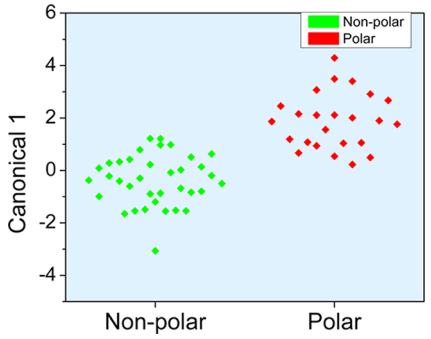

Figure 10. DFA results separating the polar material (octanol, decanol) from the non-polar material (hexane, octane, decane) at different concentrations (p_a/p_0 = 0.05, 0.1, 0.2), both in 5% and in 40% RH. Each value is the average of two repeated exposures under the same conditions.

The separation between polar and non-polar non-aromatic compounds was less accurate than the separation between aromatic and non-aromatic compounds. Other combinations of sensing features provided even lower accuracy (see Table S2, Supporting Information). Using a combination of all sensing features from all sensors and all provided better results than using either the features from one separate sensor (see Table S2b, Supporting Information) or some of the sensors (see Table S2a, Supporting Information).

After separating the polar and non-polar non-aromatic compounds, we tested the array's ability to differentiate specific VOCs in each group. In the aromatic group (see Figure 11a), the separation is based on eight parameters: $\Delta I/I_0$ of PAH-2 and -7; $\Delta V_{th}/V_{th0}$ of PAH-2 and -7; and $\Delta\mu_h/\mu_{h0}$ of PAH-2, -3, -4, and -7. The resulting accuracy was 75%. Again, all the sensors and all the sensing features were needed for the separation. It is reasonable to assume that the high absorbance of the aromatic VOCs makes them easy to discriminate from the other VOCs. However, identifying the separate aromatic VOCs would be more difficult. Figure 11a shows that the analytes were mostly separated along the negative axis of the first canonical variable, according to their polarity (except for ethyl benzene). The least polar analyte, mesitylene, has the least negative CV1 values; toluene, the most polar analyte, has the most negative CV1 value. No clear separation is seen 5% RH and the 40% RH of the same analyte, perhaps being an indication that the separation is less sensitive to humidity changes. Table S3 of the Supporting Information shows that a combination of all sensing features from all sensors provides the highest accuracy of discrimination.

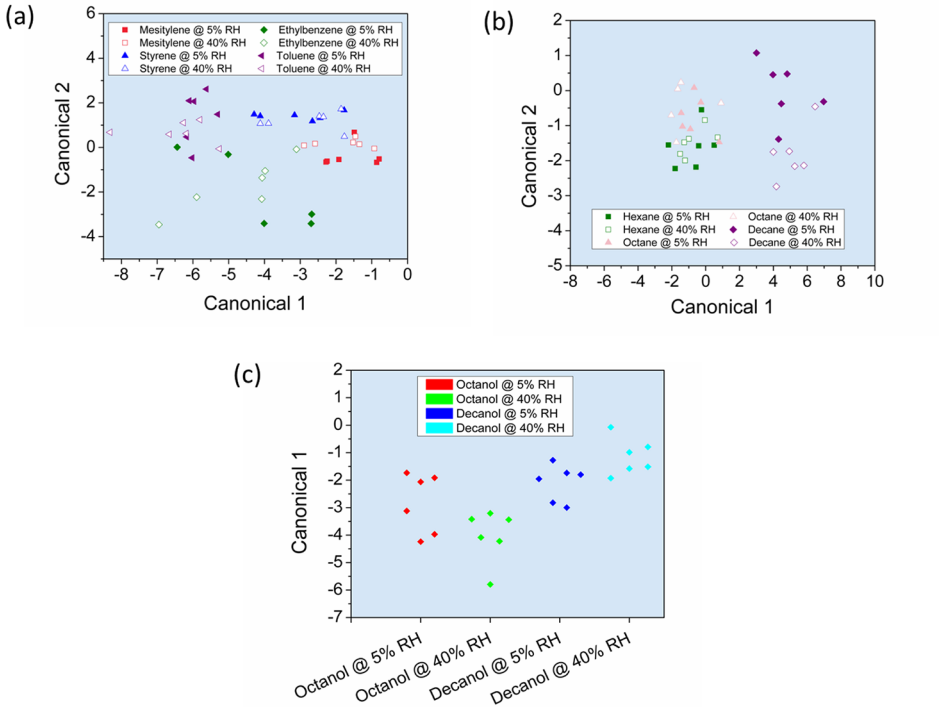

Figure 11. DFA results separating: (a) aromatic material (mesitylene, styrene, ethyl benzene, toluene); (b) non-polar VOCs (hexane, octane, decane); and (c) polar materials (octanol, decanol). The various dots stand for the response of the device upon exposure to different concentrations (p_a/p_0 = 0.05, 0.1, 0.2) of the different VOCs in both 5 and 40% RH. Each value is the average of two repeated exposures under the same conditions.

Figure 11b shows the separation different VOCs in the non-polar group (hexane, octane, and decane). The accuracy obtained was 75% and was based on six parameters ($\Delta I/I_0$ of PAH-3 and -7, $\Delta V_{th}/V_{th0}$ of PAH-3 and -7, and $\Delta\mu_h/\mu_{h0}$ of PAH-3 and -4). Decane was separated from the rest of the analytes along the axis of the first canonical variable alone, while hexane and octane were separated along the axis of the second canonical variable. As before, no significant difference could be noticed between 5% RH and 40% RH. The combination that gave the best separation did contain features from the PAH-2 sensor but included all four types of features to receive an accuracy of 75%. The same accuracy was achieved by using all the sensors in the combinations presented in Table S4a in the Supporting Information. By including more sensing features in the analysis, we can reduce, in this case, the number of sensors in the array and still achieve the same accuracy. When comparing the accuracy of the combination used in Table S4c of the Supporting Information to the accuracy in the separation chosen for non-polar VOCs, we observed that better results could be achieved by using less sensors but extracting more sensing features per sensor.

Previously, the same PAH molecules were utilized in chemiresistors[27] which could provide only one independent sensing feature. Using chemiresistors based on three types of PAHs, the same VOCs at similar concentrations (varying from $p_a/p_0 = 0.04$ and up to $p_a/p_0 = 1$) could be distinguished with an accuracy of 71%. In the present work, an array of three PAH-FETs based on PAH-3, -4, and -7 yielded a higher separation accuracy (75%). It should be noted that the highest concentration we used was $p_a/p_0 = 0.2$, while in previous studies it was $p_a/p_0 = 1$ (the higher the concentration, the easier to separate the different analytes). Since FET arrays allow extracting more independent sensing features per sensor, their discriminative power is superior, while using the same number or fewer sensors. Instead of including another kind of device to improve the sensing abilities of the array, we can exploit another feature of the same sensor for improved sensing.

Figure 11c shows the separation of the polar group (between octanol and decanol); analysis is based on four parameters: $\Delta I/I_0$ of PAH-3 and -4 and $\Delta\mu_h/\mu_{h0}$ of PAH-2 and -3; the accuracy of separation is ~80% (see Supporting Information, Table S5. The two analytes were separated along the canonical-1 axis. In contrast to sensing non-polar VOCs (using PAH-3, -4, and -7), sensing the polar VOC analysis required substituting the PAH-7 sensor (non-polar aliphatic side group) with the PAH-2 sensor (polar ester side group). This indicates that controlling the side groups controls the adsorption of the VOCs, thus affecting the sensing abilities. The PAH-FET array was more sensitive to polar analytes (79% accuracy of separation) than non-polar ones (75% accuracy of separation). This was possibly due to screening against the absorption of the non-polar analytes by the mostly polar side groups of the PAH molecules.

When analyzing the sensing abilities of the PAH-FET array, it is important to clarify that the different responses of the sensors are due to the chemistry of the organic semiconductor rather than the surface coverage. It was previously reported that the signals of the sensors to different analytes can be controlled by changing the surface coverage of the sensing material. Hence, a sensor array based on layers of the same PAH molecule, but with different surface coverage, could be created.[29] The surface coverage of our sensors is in the following order: PAH-4 > PAH-7 > PAH-3 > PAH-2. The accuracy of separation of each sensor was calculated with the leave-one-out method by choosing all three sensing features from each sensor and basing the discrimination on it alone. The order of accuracy when trying to separate, for example, the polar analytes from the non-polar ones is PAH-3 and -4 > PAH-2 > PAH-7, meaning PAH-3 and -4 gave the most accurate separation. When trying to separate the aromatic analytes, the accuracy achieved was in the following order: PAH-7 > PAH-3 > PAH-2 > PAH-4. Comparing the orders of accuracy shows that there is no correlation surface coverage and the sensing abilities of the sensors. Furthermore, it is incorrect to declare a certain sensor to have greater sensing abilities than another, since the sensitivity of each device changes as a result of the separation required. An array's separation capability is based on the properties of the sensing layer and the analytes and the mechanism applied two factors.

SUMMARY AND CONCLUSIONS

We have demonstrated the feasibility of PAH-FET sensors for VOC sensing applications in humid atmospheres. The ability to extract multiple electrical features as well as multiple signal features from each PAH-FET sensor provided a reservoir of sensing signals that allowed discrimination between aromatic and non-aromatic VOCs, discrimination between polar and non-polar non-aromatic compounds, and identification of specific VOCs within the subgroups (i.e., aromatic compounds, polar non-aromatic compounds, and non-polar non-aromatic compounds) at both low and high RH levels. So far, the multiplicity of sensing features extracted from PAH-FET sensors provides superior performances as compared with similar PAH materials that are integrated within chemiresistive platforms (or FET at $V_g = 0$). In a few cases, one could expect that a single PAH-FET sensor would demonstrate a similar performance to an array of chemiresistive sensors that are based on the same PAH layer. This result is of great importance for the construction of miniaturized, self-learning sensing systems that can work independently under real, confounding factors. Using the PAH-FET sensors, it would be possible to exchange information and construct a miniaturized model of some environmental properties under observation. Such a model could then be used to classify events of interest and take action on the basis of a high-level representation of the system context. This would allow large-scale information and communication systems using the model to autonomously adapt to highly dynamic and open environments. Ultimately, the results presented here could lead to the development of cost-effective, lightweight, low-power, noninvasive tools for the widespread detection of VOCs in real-world applications, including, but not confined to, environmental, security, food industry, health-related, and breath analysis disease diagnostics. A study for understanding the structure−property relationship PAH corona and PAH substituent functionality and the VOC chemical nature is underway and will be published elsewhere.

ASSOCIATED CONTENT

Supporting Information

Scanning electron microscopy images of FET surfaces of the different PAHs after the exposure experiments; non-normalized sensing features upon increasing the concentration of ethyl benzene in 5% RH as a function of time; and accuracy of discrimination between various groups and various types of VOCs, using different combinations of sensors and electrical features. This material is available free of charge via the Internet at http://pubs.acs.org.

AUTHOR INFORMATION

Corresponding Author

*E-mail: hhossam@tx.technion.ac.il.

Notes

The authors declare no competing financial interest.

ACKNOWLEDGMENTS

The research leading to these results has received partial funding from the FP7's ERC grant under DIAG-CANCER (grant agreement no. 256639). We acknowledge Mr. A'laa Garaa, Mr. Rawi Dirawi, Dr. Ulrike (Mirjam) Tisch, Dr. Greogory Shuster, Dr. Bin Wang, Dr. Yael Zilberman, Ms. Nisreen Shehada (Technion IIT), Mr. Nadav Bachar and Dr. Radu Ionescu (Tarragona University) for assistance and fruitful discussions.

REFERENCES

(1) Wallace, L.; Pellizzari, E.; Leaderer, B.; Zelon, H.; Sheldon, L. *Atmos. Environ.* **1987**, *21*, 385−393.
(2) Guo, H.; Lee, S.; Chan, L.; Li, W. *Environ. Res.* **2004**, *94*, 57−66.
(3) Hakim, M.; Broza, Y. Y.; Barash, O.; Peled, N.; Phillips, M.; Amann, A.; Haick, H. *Chem. Rev.* **2012**, *112*, 5949−5966.
(4) Tisch, U.; Billan, S.; Ilouze, M.; Phillips, M.; Peled, N.; Haick, H. *CML - Lung Cancer* **2012**, *5*, 107−117.
(5) Tisch, U.; Haick, H. *Rev. Chem. Eng.* **2010**, *26*, 171−179.
(6) Peled, N.; Hakim, M.; Tisch, U.; Bunn, P. A. J. R.; Miller, Y. E.; Kennedy, T. C.; Mattei, J.; Mitchell, J. D.; Weyant, M. J.; Hirsch, F. R.; Haick, H. *J. Thorac. Oncol.* **2012**, *7*, 1528−1533.
(7) Peng, G.; Hakim, M.; Broza, Y. Y.; Billan, S.; Abdah-Bortnyak, R.; Kuten, A.; Tisch, U.; Haick, H. *Br. J. Cancer* **2010**, *103*, 542−551.
(8) Peng, G.; Tisch, U.; Adams, O.; Hakim, M.; Shehada, N.; Broza, Y. Y.; Billan, S.; Abdah-Bortnyak, R.; Kuten, A.; Haick, H. *Nat. Nanotechnol.* **2009**, *4*, 669−673.
(9) Hakim, M.; Billan, S.; Tisch, U.; Peng, G.; Dvrokind, I.; Marom, O.; Abdah-Bortnyak, R.; Kuten, A.; Haick, H. *Br. J. Cancer* **2011**, *104*, 1649−1655.
(10) Barash, O.; Peled, N.; Tisch, U.; Bunn, P. A.; Hirsch, F. R.; Haick, H. *Nanomedicine (New York, NY, U.S.)* **2012**, *8*, 580−589.
(11) Barash, O.; Peled, N.; Hirsch, F. R.; Haick, H. *Small* **2009**, *5*, 2618−24.
(12) Amal, H.; Ding, L.; Liu, B. B.; Tisch, U.; Xu, Z.-Q.; Shi, D.-Y.; Zhao, Y.; Chen, J.; Sun, R.-X.; Liu, H.; Ye, S. L.; Tang, S. L.; Haick, H. *Int. J. Nanomed.* **2012**, *7*, 4135−4146.
(13) Haick, H.; Hakim, M.; Patrascua, M.; Levenberg, C.; Shehada, N.; Nakhoul, F.; Abassi, Z. *ACS Nano* **2009**, *3*, 1258−1266.
(14) Marom, O.; Nakhoul, F.; Tisch, U.; Shiban, A.; Abassi, Z.; Haick, H. *Nanomedicine (London, U.K.)* **2012**, *7*, 639−650.
(15) Tisch, U.; Aluf, A.; Ionescu, R.; Nakhle, M.; Bassal, R.; Axelrod, N.; Robertman, D.; Tessler, Y.; Finberg, J. P. M.; Haick, H. *ACS Chem. Neurosci.* **2012**, *3*, 161−166.
(16) Tisch, U.; Schlesinger, I.; Ionescu, R.; Nassar, M.; Axelrod, N.; Robertman, D.; Tessler, Y.; Marmur, A.; Aharon-Peretz, J.; Haick, H. *Nanomedicine (London, U.K.)* **2013**, *8* (1), 43−56.
(17) Ionescu, R.; Broza, Y.; Shaltieli, H.; Sadeh, D.; Zilberman, Y.; Feng, X.; Glass-Marmor, L.; Lejbkowicz, I.; Müllen, K.; Miller, A.; Haick, H. *ACS Chem. Neurosci.* **2011**, *2*, 687−693.
(18) Tisch, U.; Haick, H. *MRS Bull.* **2010**, *35*, 797−803.
(19) Konvalina, G.; Haick, H. *ACS Appl. Mater. Interfaces* **2012**, *4*, 317−325.
(20) Bondavalli, P.; Legagneux, P.; Pribat, D. *Sens. Actuat. B* **2009**, *140*, 304−318.
(21) Vlachos, D. S.; Skafidas, P. D.; Avaritsiotis, J. N. *Sens. Actuat. B* **1995**, *25*, 491−494.
(22) Li, D.; Borkent, E. J.; Nortrup, R.; Moon, H.; Katz, H.; Bao, Z. *Appl. Phys. Lett.* **2005**, *86*, 0421051−3.
(23) Pacher, P.; Lex, A.; Eder, S.; Trimmel, G.; Slugovc, C.; List, E.; Zojer, E. *Sens. Actuat. B* **2010**, *145*, 181−184.
(24) Righettoni, M.; Tricoli, A.; Gass, S.; Schmid, A.; Amann, A.; Pratsinis, S. *Anal. Chim. Acta* **2012**, *738*, 69−75.
(25) Potyrailo, R.; Nagraj, N.; Surman, C.; Boudries, H.; Lai, H.; Slocik, J. M.; Kelley-Loughnane, N.; Naik, R. R. *Trends Anal. Chem.* **2012**, *40*, 133−145.
(26) Bachar, N.; Mintz, L.; Zilberman, Y.; Ionescu, R.; Feng, X.; Mü llen, K.; Haick, H. *ACS Appl. Mater. Interfaces* **2012**, *4*, 4960−4965.
(27) Zilberman, Y.; Ionescu, R.; Feng, X.; Mullen, K.; Haick, H. *ACS Nano* **2011**, *5*, 6743−6753.
(28) Zilberman, Y.; Tisch, U.; Pisula, W.; Feng, X.; Mullen, K.; Haick, H. *Langmuir* **2009**, *25*, 5411−5416.
(29) Zilberman, Y.; Tisch, U.; Shuster, G.; Pisula, W.; Feng, X.; Mullen, K.; Haick, H. *Adv. Mater.* **2010**, *22*, 4317−4320.
(30) Torsi, L.; Dodabalapur, A.; Savvatini, L.; Zambonin, P. G. *Sens. Actuators, B* **2000**, *67*, 312−316.
(31) Li, B.; Lambeth, D. N. *Nano Lett.* **2008**, *8*, 3563−3567.
(32) Paska, Y.; Haick, H. *J. Phys. Chem. C* **2009**, *113*, 1993−1997.
(33) Paska, Y.; Haick, H. *Appl. Phys. Lett.* **2009**, *95*, 233103/1.
(34) Paska, Y.; Haick, H. *J. Am. Chem. Soc.* **2010**, *132*, 1774−1775.
(35) Paska, Y.; Haick, H. *ACS Appl. Mater. Interfaces* **2012**, *4*, 2604−2617.
(36) Paska, Y.; Stelzner, T.; Assad, O.; Tisch, U.; Christiansen, S.; Haick, H. *ACS Nano* **2012**, *6*, 335−345.
(37) Paska, Y.; Stelzner, T.; Christiansen, S.; Haick, H. *ACS Nano* **2011**, *5*, 5620−5626.
(38) Feng, X.; Pisula, W.; Kudernac, T.; Wu, D.; Linjie, Z.; Feyter, S.; Müllen, K. *J. Am. Chem. Soc.* **2009**, *131*, 4439−4448.
(39) Feng, X. L.; Pisula, W.; Zhi, L. J.; Takase, M.; Müllen, K. *Angew. Chem., Int. Ed.* **2008**, *47*, 1703−1706.
(40) Feng, X. L.; Liu, M. Y.; Pisula, W.; Takase, M.; Li, J. L.; Müllen, K. *Adv. Mater.* **2008**, *14*, 2684−2689.
(41) Bashouti, M. Y.; Tung, R. T.; Haick, H. *Small* **2009**, *5*, 2761−2769.
(42) Haynes, W. M. *CRC Handbook of Chemistry and Physics*, 91st ed.; CRC Press: Boulder, CO, 2010−2011.